© 2017. Published by The Company of Biologists Ltd | Journal of Experimental Biology (2017) 220, 2036-2046 doi:10.1242/jeb.156281

RESEARCH ARTICLE

Ontogeny of bite force in a validated biomechanical model of the American alligator

Kaleb C. Sellers[1,*], Kevin M. Middleton[1], Julian L. Davis[2] and Casey M. Holliday[1]

ABSTRACT

Three-dimensional computational modeling offers tools with which to investigate forces experienced by the skull during feeding and other behaviors. American alligators (*Alligator mississippiensis*) generate some of the highest measured bite forces among extant tetrapods. A concomitant increase in bite force accompanies ontogenetic increases in body mass, which has been linked with dietary changes as animals increase in size. Because the flattened skull of crocodylians has substantial mediolaterally oriented muscles, crocodylians are an excellent model taxon in which to explore the role of mediolateral force components experienced by the feeding apparatus. Many previous modeling studies of archosaur cranial function focused on planar analysis, ignoring the mediolateral aspects of cranial forces. Here, we used three-dimensionally accurate anatomical data to resolve 3D muscle forces. Using dissection, imaging and computational techniques, we developed lever and finite element models of an ontogenetic series of alligators to test the effects of size and shape on cranial loading and compared estimated bite forces with those previously measured *in vivo* in *A. mississippiensis*. We found that modeled forces matched *in vivo* data well for intermediately sized individuals, and somewhat overestimated force in smaller specimens and underestimated force in larger specimens, suggesting that ontogenetically static muscular parameters and bony attachment sites alone cannot account for all the variation in bite force. Adding aponeurotic muscle attachments would likely improve force predictions, but such data are challenging to model and integrate into analyses of extant taxa and are generally unpreserved in fossils. We conclude that anatomically accurate modeling of muscles can be coupled with finite element and lever analyses to produce reliable, reasonably accurate estimate bite forces and thus both skeletal and joint loading, with known sources of error, which can be applied to extinct taxa.

KEY WORDS: Crocodylia, Biomechanics, Feeding, Finite element analysis, Modeling

INTRODUCTION

Developing computational models that accurately estimate biological and biomechanical functions remains difficult for researchers interested in complex systems such as the feeding apparatus of vertebrates. Even modeling superficially simple systems such as the akinetic, two-part skull of crocodylians poses challenges given the complex, 3D nature of the bones and the jaw muscles that actuate them. Nonetheless, accurately characterizing the biomechanical performance of the feeding apparatus is critical to our understanding of the evolution of the skull. Many modeling techniques have been advanced in recent years, such as finite element analysis (FEA), multi-body dynamic analysis and BoneLoad (Davis et al., 2010), but the predictions generated by these techniques often remain to be validated by comparisons with *in vivo* data. Validated modeling may be used to carry out *in silico* experimental investigations into the performance of the feeding apparatus in extant taxa. Moreover, the use of validated models is critical to studies of form and function in fossil taxa.

The feeding apparatus of extant crocodylians produces the highest measured bite forces among extant tetrapods (Erickson et al., 2003). Counter-intuitively, crocodylians do not display the typical morphology of other hard-biting tetrapods such as tegu lizards, hyenas or *Tyrannosaurus*, in which the skull is dorsally heightened, expanding the attachment area of temporal muscles and resisting dorsoventral bending of the rostrum (Molnar, 1998; Metzger and Herrel, 2005; Tseng and Stynder, 2011; Schaerlaeken et al., 2012). Instead, crocodylians evolved a dorsoventrally flattened skull, which is hypothesized to be an adaptation for aquatic ambush predation (Iordansky, 1973). This configuration is associated with a suite of biomechanical modifications of the feeding apparatus. The consequences of this flattened skull include a shift in temporal muscles toward more mediolateral orientations as well as increased resistance to mediolateral bending and axial torsion of the cranium (Busbey, 1995). The discordance between the morphology of the crocodylian skull and that of most animals with hard bites suggests that study of the former group can yield valuable insights into the anatomical determinants of feeding performance.

The morphology and performance of the crocodylian feeding apparatus have been the focus of numerous investigations over the past century. The early comparative and functional morphological studies of Iordansky (1964) and Langston (1973) set the stage for more quantitative biomechanical investigations of the crocodylian feeding apparatus such as the functional morphological investigations of Sinclair and Alexander (1987), Busbey (1989, 1995) and Cleuren et al. (1995). These early works used 2D static equilibrium lever analyses to estimate the magnitude and orientation of bite force and joint forces in the parasagittal plane. More recently, advances in computational power have facilitated *in silico* quantitative studies of feeding biomechanics. FEA provides tools to computationally investigate stress and strain (Daniel and McHenry, 2001; Metzger et al., 2005) and reaction forces (Porro et al., 2011, 2013) under a wide range of loading conditions. Researchers have applied this technique to investigate how feeding behavior loads the rostrum in comparative samples of extant crocodylians (McHenry et al., 2006; Pierce et al., 2008), comparing among archosaurs (Rayfield et al., 2007; Rayfield and Milner, 2008), and extinct crocodylomorphs such as thalattosuchians (Pierce et al., 2009). Using multi-body dynamics,

[1]Department of Pathology and Anatomical Sciences, University of Missouri, M263, Medical Sciences Building, Columbia, MO 65212, USA. [2]Department of Engineering, University of Southern Indiana, 2030 Business and Engineering Center, 8600 University Boulevard, Evansville, IN 41172, USA.

*Author for correspondence (kcsty5@mail.missouri.edu)

K.C.S., 0000-0002-3588-9562

Received 11 January 2017; Accepted 15 March 2017

Journal of Experimental Biology

Journal of Experimental Biology (2017) 220, 2036-2046 doi:10.1242/jeb.156281

List of symbols and abbreviations

3D LM	three-dimensional lever mechanics
A_{ins}	area of muscle insertion (mandibular attachment)
A_{or}	area of muscle origin (cranial attachment)
$\mathbf{F}_B$	bite force vector
FEA	finite element analysis
F_M	muscle force magnitude
$\mathbf{F}_M$	muscle force vector
l_f	fiber length
l_M	muscle length
mAMEM	M. adductor mandibulae externus medialis
mAMEP	M. adductor mandibulae externus profundus
mAMES	M. adductor mandibulae externus superficialis
mAMP	M. adductor mandibulae posterior
mDM	M. depressor mandibulae
mPSTp	M. pseudotemporalis profundus
mPSTs	M. pseudotemporalis superficialis
mPTd	M. pterygoideus dorsalis
mPTv	M. pterygoideus ventralis
$\mathbf{M}_{JJA}$	magnitude of moment about jaw joint axis
PCSA	physiological cross-sectional area
$\mathbf{r}_B$	position vector of bite force
$\mathbf{r}_M$	position vector of muscle force vector
$T_{specific}$	specific tension of muscle
$\mathbf{u}_{JJA}$	unit vector of jaw joint axis
V_M	muscle volume
θ	pennation angle

Bates and Falkingham (2012) compared estimates of bite force of *Tyrannosaurus* with estimates from various tetrapods including a large individual of *Alligator mississippiensis*. These authors found that peak (impact) bite forces in *A. mississippiensis* matched previously reported maximum *in vivo* data.

Numerous *in vivo* studies have provided crucial data and advanced our understanding of the performance of the feeding apparatus in crocodylians. Researchers using electromyography (EMG) and X-ray cineradiography found that all major groups of adductor muscles were active during crushing bites but showed that the pterygoideus muscles were inactive during holding bites (Van Drongelen and Dullemeijer, 1982; Busbey, 1989; Cleuren and de Vree, 1992; Cleuren et al., 1995). Metzger et al. (2005) measured *in vivo* strain in the cranium during biting and found that these data broadly agreed with computational predictions. Most recently, Porro et al. (2013) found that *in vivo* strain magnitudes in the mandibles generally surpass predictions from FEA.

In vivo bite force recordings using force transducers are an invaluable source of data for further understanding the ontogenetic scaling and comparative biomechanics of the crocodylian feeding apparatus. Erickson and colleagues conducted a series of studies that measured bite force in a growth series of American alligator (Erickson et al., 2003; Gignac and Erickson, 2015) and extant crocodylian species (Erickson et al., 2012, 2014). Across a size range of 31.5 to 405.5 cm total length, these studies found a positive allometric relationship (b) between maximum bite force and a variety of body size proxies, such as total length (b=2.62; isometry=2), snout–vent length (b=2.59; isometry=2), mass (b=0.79; isometry=0.667) and head length (b=2.75; isometry=2). Erickson et al. (2003) hypothesized that this positively allometric increase in bite force may be responsible for intraspecific niche partitioning in *A. mississippiensis*. Furthermore, with the exception of *Gavialis gangeticus*, all extant crocodylians of a given size have equivalent bite forces. These studies have provided a solid *in vivo* basis against which *in silico* predictions may be tested.

Gignac and Erickson (2016) compared estimates of *A. mississippiensis* bite force derived from static bite force modeling with their previously published *in vivo* findings. The modeling techniques employed by the authors reliably calculate bite force in *A. mississippiensis*. These authors used photographs of dissections to precisely measure muscular physiological cross-sectional area (PCSA). Although this method is successful in calculating bite force in *A. mississippiensis*, it relies on access to cadaveric specimens, and, as such, is not applicable to the fossil record.

Although most previous modeling studies investigated the effects of muscle force on cranial forces in the skulls of crocodylians, few relied on anatomically detailed muscular attachment geometry from

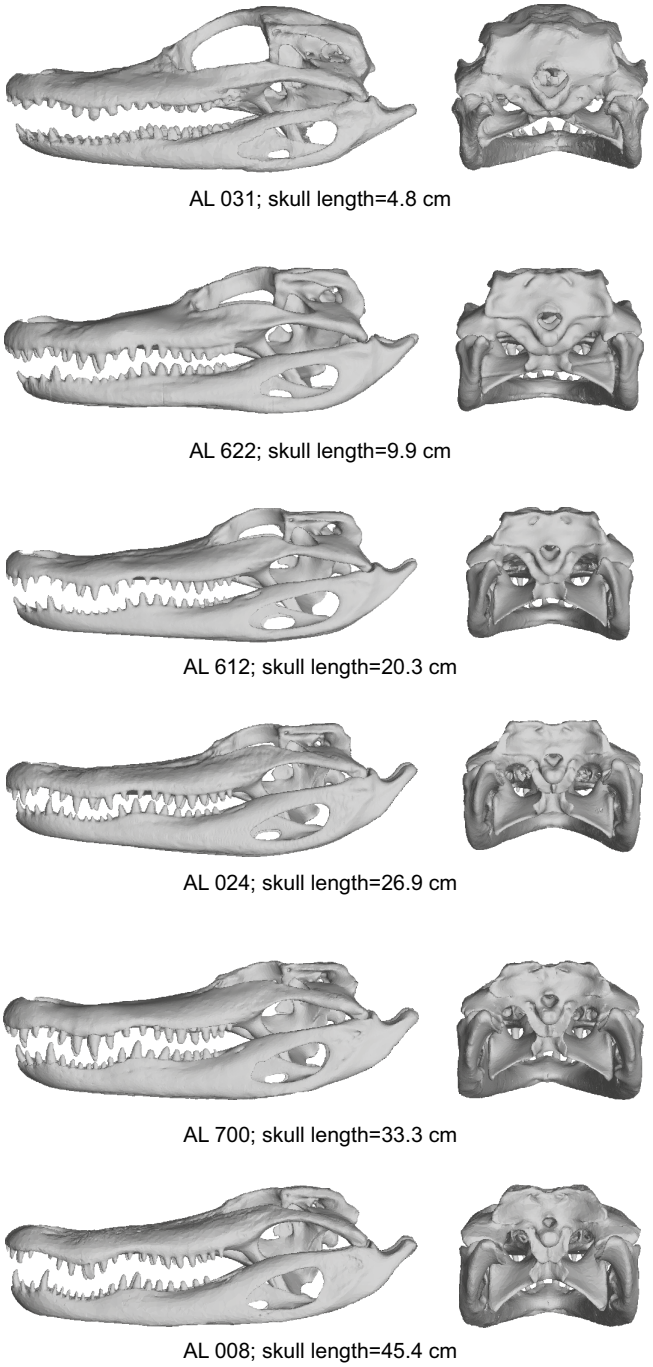

Fig. 1. Left lateral (left) and caudal (right) views of modeled *Alligator mississippiensis* specimens. All models are scaled to the same skull length.

Journal of Experimental Biology (2017) 220, 2036-2046 doi:10.1242/jeb.156281

an ontogenetic series of animals. Of course, some studies of extant crocodylian biomechanics have benefited from dissection of cadaveric specimens to inform muscle force reconstructions (Porro et al., 2011; Gignac and Erickson, 2016), but these methods are not immediately applicable to questions of cranial function in extinct crocodyliforms. As such, accurate methods for muscle modeling in fossil taxa should be pursued to better understand the evolution of this system. Thus, despite the long history of functional analyses of crocodylian skulls, our understanding of the biomechanical environment of the feeding apparatus requires improvement.

Here, we tested the hypothesis that bite force predictions using digital models of skull morphology, myology and 3D computational modeling will be consistent with *in vivo* data. Specifically, we hypothesized that our model will generate bite forces consistent with the positively allometric relationship previously reported in *in vivo* bite force data from an ontogenetic series of *A. mississippiensis* (Erickson et al., 2003). Bite force was calculated using 3D lever mechanics and FEA. Although finite element software was used to create models, map muscle attachment sites and interface with BoneLoad in order to distribute muscle forces, we used FEA to calculate bite force; we did not investigate stress or strain distributions or deformation in the present study. Barring biologically unrealistic deformation, forces calculated with FEA should converge with results obtained with 3D lever mechanics.

MATERIALS AND METHODS

Specimens and model construction

Five frozen, unpreserved specimens of *A. mississippiensis* Daudin 1802 were obtained from Rockefeller Wildlife Refuge (Grand Chenier, LA, USA), and a single dry skull was obtained from a private collector. Skull lengths ranged from 4.8 to 45.4 cm (Fig. 1, Table 1), corresponding to total body lengths of approximately 38–326 cm (Woodward et al., 1995). The smallest individual was CT scanned at the University of Missouri Biomolecular Imaging Center (Siemens Inveon MicroCT, Siemens Medical Solutions USA Inc., Malvern, PA, USA); the largest individual was scanned at the University of Missouri School of Medicine Department of Radiology (Siemens Somatom Definition Scanner, Siemens Medical Solutions USA Inc.). All other animals were scanned at the University of Missouri School of Veterinary Medicine (GE LightSpeed VCT CT scanner, GE Medical, Milwaukee, WI, USA).

Stacked images were manually segmented in Avizo 9 (Visualization Sciences Group, SAS, Merignac, France; Fig. 2A), and three-dimensional models of skeletal anatomy were created (Fig. 2B). Using Geomagic Studio 13 (Geomagic Inc., Research Triangle Park, NC, USA), models were aligned to world axes and cleaned to remove features that unnecessarily increased computational time. Meshes were constructed with four-noded tetrahedra in Strand7 (G1D Computing Pty Ltd, Sydney, Australia; Fig. 2C). Four-noded tetrahedral bricks were used to construct finite element models. Finally, muscle attachments were 'mapped' onto the models using Strand7 following the methods of Grosse et al. (2007; Fig. 2D). All models had at least 500,000 elements to ensure models behaved convergently (McCurry et al., 2015; Table S1). The dimensions of the models are: x is positive in the left lateral direction, y is positive in the dorsal direction and z is positive in the rostral direction. All models were tested at 5 deg of gape. Finite element models are available online (https://osf.io/jmpck/). We modeled unilateral, left-sided, static, crushing bites at the most caudally located maxillary tooth, where bite force is theoretically highest and where Erickson et al. (2003) measured bite force. Muscles were assumed to contract maximally, as reported by previous EMG studies (Busbey, 1989; Cleuren et al., 1995).

Table 1. *Alligator mississippiensis* specimens, skull length, scan data and model data

Specimen	Skull length (cm)	Pixel size (mm)	Interslice spacing (mm)	Tetrahedron no. (skull)
AL 031	4.8	0.083374	0.083374	612,061
AL 622	9.9	0.16	0.5	1,242,107
AL 612	20.3	0.25	0.5	988,762
AL 024	26.9	0.429689	0.625	967,293
AL 700	33.3	0.51	0.5	1,313,622
AL 008	45.4	0.570313	0.6	613,219

Muscle modeling

Calculations of bite force using both 3D lever mechanics (3D LM) and FEA require either direct measurements or accurate estimations of the force of muscular contraction. Muscles generate force in proportion to PCSA (Gans, 1982). PCSA is a function of muscle volume, fiber length (in terms of fractions of total muscle length) and muscle pennation (Gans, 1982). Because cross-sectional area is challenging to measure, volume is divided by fiber length to

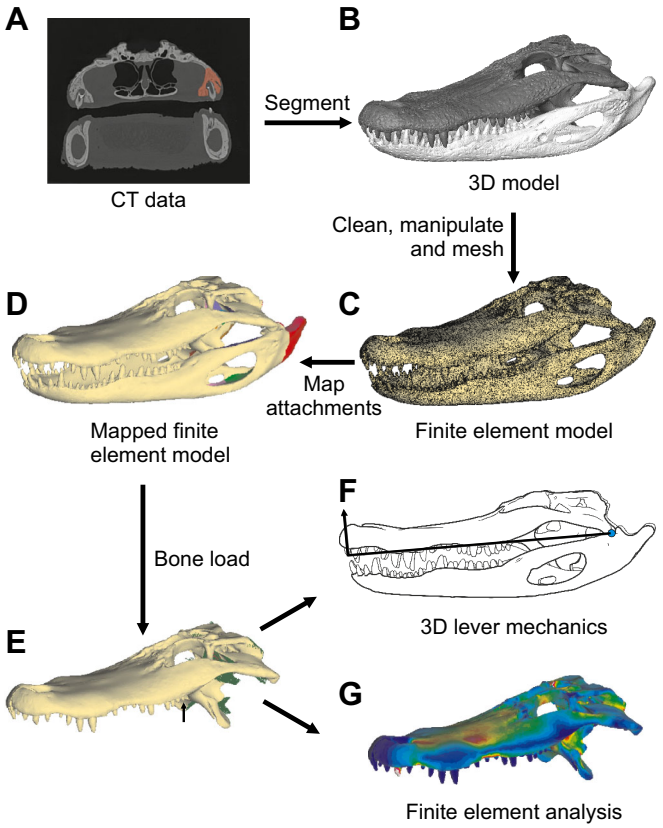

Fig. 2. Workflow of model creation and analysis. (A) Raw CT scans were segmented manually. (B) Manual segmentation data were used to generate a 3D model. (C) Models were cleaned, manipulated to the same gape, and meshed to create finite element models. (D) Bony muscle attachment sites were mapped to surfaces of the model. (E) The computational package BoneLoad (Davis et al., 2010) was used to distribute muscle forces across attachment sites. Bite point is indicated with a vertical arrow. 3D lever mechanics (F) and finite element analysis (G) were used to calculate bite forces.

Journal of Experimental Biology

Journal of Experimental Biology (2017) 220, 2036-2046 doi:10.1242/jeb.156281

estimate cross-sectional area, as defined in Eqn 1 (Sacks and Roy, 1982):

$$\mathrm{PCSA} = \frac{V_\mathrm{M}}{l_\mathrm{f}} \cdot \cos(\theta), \quad (1)$$

where V_M is muscle volume, l_f is the fiber length of the muscle and θ is the angle of pennation. Fiber length and pennation data are from Porro et al. (2011). As a goal of this study was to validate a method with applicability to the fossil record, we chose to calculate PCSA by estimating muscle volume from the surface area of attachment sites rather than from measured muscle volume. Muscle volumes were therefore estimated by treating each muscle as a frustum, a cone with its apex cut off parallel with its base. Eqn 2 defines the volume of a frustum:

$$V_\mathrm{M} = \frac{l_\mathrm{M}}{3} \cdot (A_\mathrm{or} + A_\mathrm{ins} + \sqrt{A_\mathrm{or} \cdot A_\mathrm{ins}}), \quad (2)$$

where l_M is the length of the muscle, A_or is the surface area of the origin of the muscle and A_ins is the surface area of its insertion. Muscle attachment sites were mapped onto finite element models in Strand7. Because of small variations in mesh construction, muscle attachment areas were not always perfectly symmetrical but never differed by more than 5%. Dissections and reference to the literature (Iordansky, 1964, 2000; Schumacher, 1973; Busbey, 1989; Holliday and Witmer, 2007; Holliday et al., 2013) guided muscle mapping. The ratio between PCSA and force produced is specific tension, defined in Eqn 3:

$$F_\mathrm{M} = \mathrm{PCSA} \cdot T_\mathrm{specific}, \quad (3)$$

where F_M is muscle force and T_specific is specific tension. Specific tension data value is from Porro et al. (2011).

All muscle terminology follows Holliday and Witmer (2007). In the present study, muscles modeled were M. adductor mandibulae externus superficialis (mAMES), M. adductor mandibulae externus medialis (mAMEM), M. adductor mandibulae externus profundus (mAMEP), M. adductor mandibulae posterior (mAMP), M. pseudotemporalis superficialis (mPSTs), M. pseudotemporalis profundus (mPSTp), M. pterygoideus dorsalis (mPTd), M. pterygoideus ventralis (mPTv) and M. depressor mandibulae (mDM). In extant crocodylians, most cranial muscles have substantial mediolateral components (mAMEM, mAMEP, mPSTp), rostrocaudal components (mPTd), or both (mAMES, mAMP, mPSTs, mPTv, mDM; Fig. 3).

In this study, muscle force was distributed over the surface area of attachment of the origin rather than modeled as a single vector. Each face of a tetrahedral element belonging to a muscle origin bore a portion of the total force, directed at the centroid of the muscle insertion. The computational toolkit BoneLoad version 7 (Davis et al., 2010) was used for distributing muscle forces across attachment sites and to calculate moments about axes. BoneLoad was originally used in modeling bite forces in phyllostomid bats, and its predictions are well supported by *in vivo* measurements (Davis et al., 2010; Santana et al., 2010). BoneLoad uses the geometry of muscle attachments (Fig. 3) and magnitude of muscle forces to automate the calculation of moments about an axis of rotation and distribute these muscular forces (Fig. 2E). These muscular force distributions were then used in both 3D lever analysis (Fig. 2F) and FEA (Fig. 2G).

3D LM

Lever systems transmit force by the rotational tendency of an element about an axis. An input force acting at a distance from this axis imparts a moment of force (a measure of rotational tendency) around the axis. A second object at a distance from the axis will experience an output force, resisting this rotational tendency. In the feeding apparatus, cranial muscles provide the input force for rotation, and the food item experiences the output force, which is realized as bite force. The perpendicular distance from the muscle force vector to the axis of rotation is the moment arm of the muscle. Eqn 4 describes the calculation of moments about the jaw joint axis (JJA):

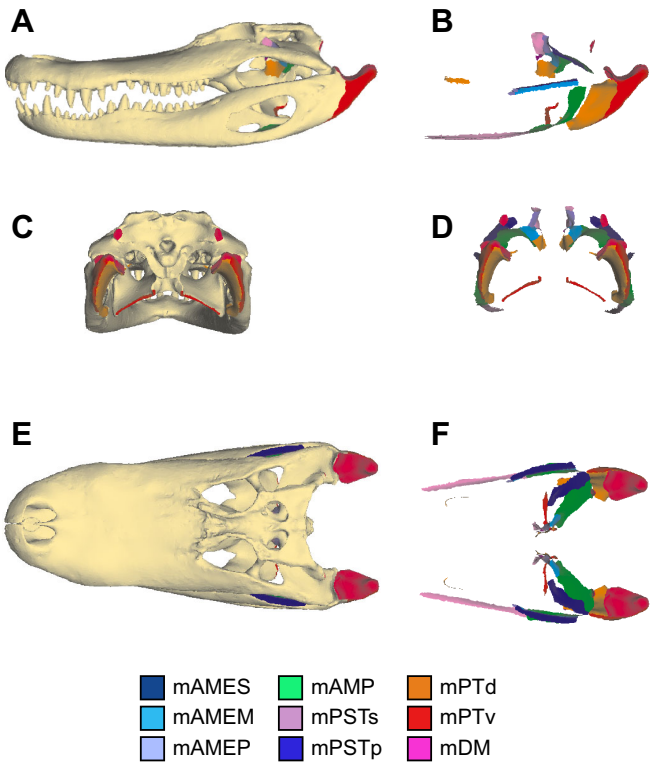

Fig. 3. Left lateral (top), caudal (middle) and dorsal (bottom) views of muscle attachments. (A,C,E) Attachment sites on bony morphology. (B,D,F) Skeleton removed to show attachment sites alone. Muscle abbreviations are as in Materials and methods.

$$\mathbf{M}_\mathrm{JJA} = \mathbf{u}_\mathrm{JJA} \cdot (\mathbf{r}_\mathrm{M} \times \mathbf{F}_\mathrm{M}), \quad (4)$$

where $\mathbf{M}_\mathrm{JJA}$ is the moment about the jaw joint axis, $\mathbf{u}_\mathrm{JJA}$ is the unit vector describing the JJA (defined as the vector passing through the middle of the joint surfaces of each articular bone), $\mathbf{r}_\mathrm{M}$ locates the muscle insertion (and thus the muscle force vector) relative to one of the jaw joints, and $\mathbf{F}_\mathrm{M}$ is the vector describing the magnitude and orientation of muscle force.

Output forces in lever systems act perpendicularly to the plane containing the axis of rotation and the output moment arm. Eqn 5 describes the relationship of moments about the jaw joint axis and bite force:

$$\mathbf{M}_\mathrm{JJA} = \mathbf{u}_\mathrm{JJA} \cdot (\mathbf{r}_\mathrm{B} \times \mathbf{F}_\mathrm{B}), \quad (5)$$

where $\mathbf{r}_\mathrm{B}$ locates the bite point relative to a jaw joint and $\mathbf{F}_\mathrm{B}$ describes the magnitude and orientation of bite force. Other variables are as in Eqn 4. By performing these calculations for each muscle, the total moment about the jaw joint axis was calculated. Bite force is then the quotient of total moments and the perpendicular distance from the bite point to the jaw joint axis. Fig. 4 illustrates the calculation of bite force using lever mechanics for a single muscle.

Journal of Experimental Biology (2017) 220, 2036-2046 doi:10.1242/jeb.156281

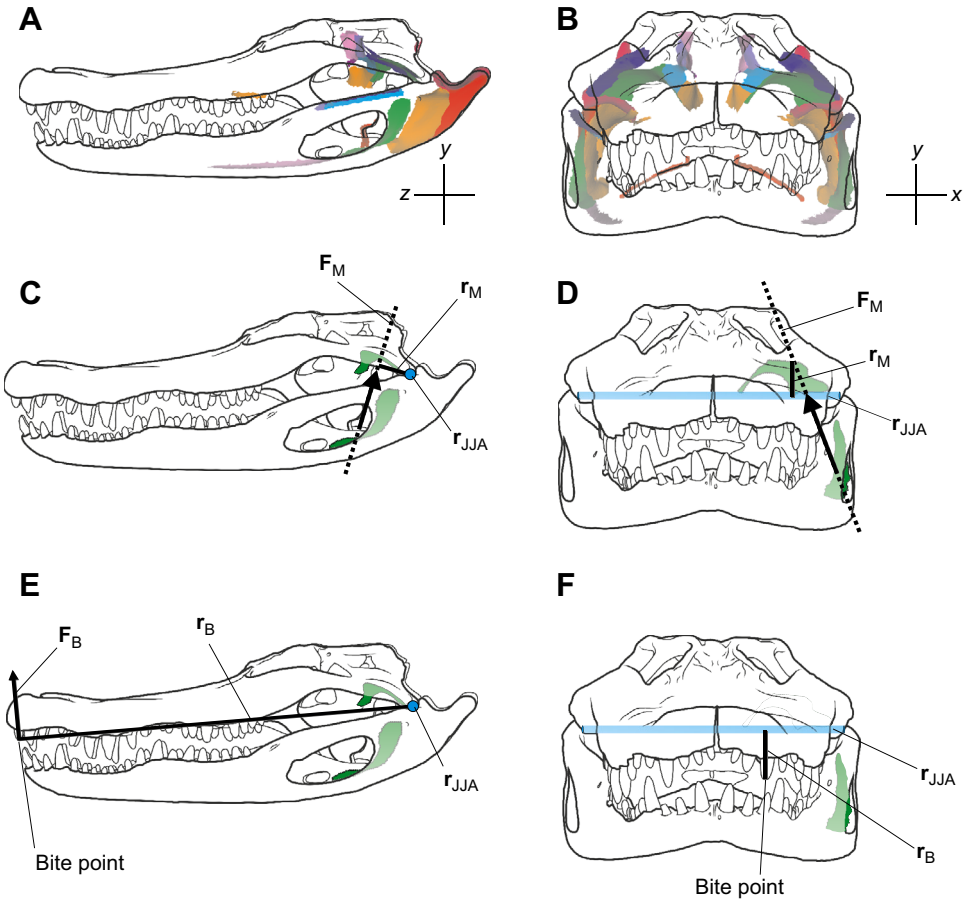

Fig. 4. 3D lever analysis. Muscle attachment colors are as in Fig. 3. Left: left lateral view. Right: rostral view. (A,B) Muscle attachments. (C,D) Calculation of moment about jaw joint axis (JJA). Attachment of adductor mandibulae posterior (mAMP) is highlighted. $\mathbf{F}_M$, muscle force; $\mathbf{r}_M$, perpendicular vector from muscle attachment site to axis of rotation; $\mathbf{r}_{JJA}$, vector between the two jaw joints. (E,F) Calculation of output (bite) force. $\mathbf{F}_B$, bite force; $\mathbf{r}_B$, perpendicular vector from axis of rotation to bite point. See Eqns 4 and 5.

FEA

Bite force was also calculated using FEA. In FEA, the user constrains the degrees of freedom at specified nodes. The FEA software then calculates the force required at each constraint to maintain equilibrium. Methods described by Strait et al. (2005) were followed to assign constraints. A single node at the tip of the caudal tooth and a single node in the middle of the articular surface of each quadrate bone were constrained in all three translational and all three rotational degrees of freedom. Material properties of alligator mandibular cortical bone were assigned to all elements of the FEM following Zapata et al. (2010). The scope of this project prohibited the inclusion of cranial sutures in the models; further, the material properties of sutures in *A. mississippiensis* (or indeed, the material properties of cranial sutures in any reptile) are unknown. Porro et al. (2011) found that although including sutures in finite element models affects stress and strain distributions in the alligator mandible, reaction forces including bite force were not dramatically affected. Although we were not investigating stress and strain distributions in the skull in the present study, we would expect artificial concentrations of stress and strain near bite points and muscle attachments (Curtis et al., 2013). For these reasons, cranial sutures were not included here. Because FEA provides force orientations, the component of force in each dimension is reported in addition to overall magnitudes (mediolateral, $\mathbf{F}_x$; dorsoventral, $\mathbf{F}_y$; rostrocaudal, $\mathbf{F}_z$; total, $\mathbf{F}_{sum}$).

Statistical analysis

Biomechanical models are useful only insofar as they produce consistent results that are at least broadly comparable with *in vivo* data. To validate this method, bite forces calculated using both 3D LM and FEA were compared with *in vivo* bite force data reported by Erickson et al. (2003). Erickson and colleagues measured maximum *in vivo* bite force in an ontogenetic series of *A. mississippiensis* using force transducers. To assess how bite forces calculated in this study correspond to *in vivo* data, ordinary least squares regression was conducted on bite force calculated with both FEA and 3D LM against skull length using R (http://www.R-project.org/). Because Erickson et al. (2003) did not report skull lengths, we used the published relationship of skull length against snout–vent length (Woodward et al., 1995) to calculate skull lengths for individuals in the study of Erickson et al. (2003). Ordinary least squares regression is justified over standardized major axis regression, because although skull lengths were presumably not measured without error, the error is likely to be low and the ratio of this error to the error in either directly measured or estimated bite force is also low. To compare slopes of regressions of log-transformed bite force on log-transformed skull length between Erickson et al.'s (2003) data and our results, we used a linear model with data source (*in vivo*, FEA and 3D LM), skull length and the interaction term. This analysis of covariance model allows each source of bite force data to have a separate slope while allowing comparison between slopes.

In the case of significantly different slopes between modeled and measured bite force data, we used the Johnson–Neyman technique to determine the region in which there is no significant difference in slope (Johnson and Neyman, 1936; White, 2003). The Johnson–Neyman technique compares two regressions and provides upper and lower values of the independent variable between which slopes do not significantly differ. We used the Johnson–Neyman technique to compare *in vivo* data with both FEA and 3D LM forces. All code for analysis is available online (https://osf.io/jmpck/).

Journal of Experimental Biology (2017) 220, 2036-2046 doi:10.1242/jeb.156281

RESULTS

Bite force typically refers only to the compressive (i.e. dorsoventral) components of force acting on a food item, as this is the component of force that will do work on food. FEA calculates forces acting in all dimensions, but lever mechanics calculates only forces acting perpendicular to the plane containing the axis of rotation and the point of force application. Similarly, the bite force transducers used by Erickson et al. (2003) measured only forces acting perpendicular to the long axis of the cantilever. In both cases, forces are dorsoventrally oriented. The results of FEA presented below therefore only include the magnitude of dorsoventral force, and statistical analyses were performed on only the dorsoventral component of bite force, which was typically ~90% of total bite force.

Model construction and muscle modeling

Regression of muscle length, volume and force against skull length showed that these parameters scaled isometrically in all muscles with the exception of mAMEP and mPSTp, in which muscle volume and force scaled with slight negative allometry (slope estimates of 1.59 and 1.52, respectively; see Table 2 and Table S1). Fig. 5 shows reconstructed muscle force and the proportion each muscle contributes to total muscle force. Note that mAMP and mPTd together account for approximately two-thirds of muscle force in our model. However, our methods likely underestimate the force of mPTv; see Discussion.

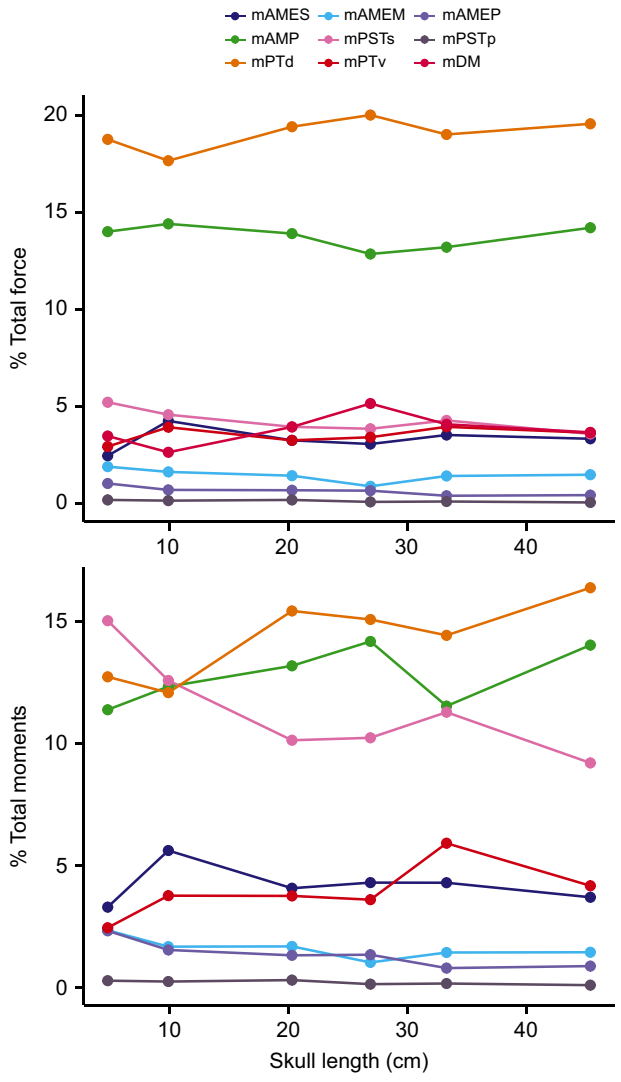

Fig. 5. Proportion each muscle contributes to total muscle force (top) and total moment about the jaw joint and therefore bite force (bottom). Muscle attachment colors are as in Fig. 3. Note that mDM opens the jaw and therefore is not included in the bottom panel. Although mPTd is consistently the strongest muscle, mPSTs contributes the most to bite force in the smaller two specimens.

3D LM and FEA

Bite force estimates ranged from 49.3 N in the smallest individual (both methods) to 3460 N in the largest individual (3D LM). Bite force estimation with 3D LM and FEA yielded nearly identical results (Table 3). Magnitudes of total bite forces calculated with FEA and 3D LM differed by <6%. Whereas bite forces calculated in intermediately sized individuals matched *in vivo* data well, bite force in larger and smaller individuals diverged from *in vivo* data, with lower force estimates in larger individuals and higher force estimates in smaller individuals relative to *in vivo* data. The percentage contribution of a muscle to bite force is not necessarily the same as its percentage contribution to total muscle force (Fig. 5; Tables 4 and 5), because muscles vary in attachment site geometry in the crocodylian adductor chamber. For comparisons with *in vivo* bite force data, we only considered the dorsoventral component of bite force. However, the conditions of static equilibrium demand that forces be balanced in all three dimensions. Therefore, our FEA also calculated rostrocaudal and mediolateral components of bite force (Table 6). Bite points experienced medially and rostrally acting forces in addition to dorsoventral force.

Statistical analysis

Regression of bite force against skull length showed that both 3D LM- and FEA-calculated bite forces do not significantly differ from isometry (3D LM 95% confidence interval 1.64–2.06; FEA 95% confidence interval 1.63–2.05). By contrast, *in vivo* data from Erickson et al. (2003) showed positive allometry (95% confidence interval 2.51–2.61). Application of the Johnson–Neyman technique on both sources of calculated bite force data against *in vivo* results of Erickson et al. (2003) revealed that both samples had a region of non-significant difference of slopes. For bite force calculated with 3D LM, median values of lower and upper skull length in the region where slopes were not significantly different were 9.8 to 17.9 cm, respectively. Between these sizes, 3D LM predicts a slope that does not significantly differ from *in vivo* data. For bite force calculated with FEA, median values of skull length were 9.5–17.4 cm (Fig. 6). Between these sizes, FEA predicts a slope that does not significantly differ from *in vivo* data.

DISCUSSION

Biomechanical modeling offers researchers powerful tools with which to test hypotheses of feeding performance of extant and extinct taxa. *In vivo* bite force data of wild crocodylians are challenging to obtain, and *in vivo* measurements are obviously not possible in extinct taxa, making computational modeling necessary to explore patterns of form and function in the group. Accurate computational methods can model biting under varying conditions of tooth contact, gape and muscle recruitment, and thus modern computational methods are an excellent option for investigating the relationship between morphology, bite force and resulting cranial forces.

Validation with *in vivo* bite force data

The two biomechanical modeling techniques used in this paper produce results consistent with each other. Like other validated

Journal of Experimental Biology (2017) 220, 2036-2046 doi:10.1242/jeb.156281

Table 2. *Alligator mississippiensis* jaw muscle forces calculated by estimating PCSA by frustum muscle modeling

	Force											
	AL 031 4.8 cm		AL 622 9.9 cm		AL 612 20.3 cm		AL 024 26.9 cm		AL 700 33.3 cm		AL 008 45.4 cm	
Muscle	(N)	(%)	(N)	(%)	(N)	(%)	(N)	(%)	(N)	(%)	(N)	(%)
L mAMES	5.45	2.48	32.6	4.32	72.8	3.31	154	3.01	287	3.46	665	3.48
R mAMES	5.39	2.45	31.6	4.20	70.5	3.21	160	3.13	299	3.61	612	3.20
L mAMEM	4.17	1.90	12.5	1.66	31.1	1.41	45.2	0.883	120	1.44	272	1.42
R mAMEM	4.20	1.91	12.1	1.61	32.2	1.47	46.3	0.905	117	1.41	298	1.56
L mAMEP	2.30	1.05	5.55	0.737	15.2	0.693	35.3	0.690	34.3	0.414	84.5	0.443
R mAMEP	2.26	1.03	5.13	0.681	15.2	0.691	33.1	0.648	33.3	0.402	83.2	0.436
L mAMP	31.6	14.4	110	14.6	309	14.1	659	12.9	1150	13.8	2720	14.2
R mAMP	30.0	13.6	107	14.2	300	13.7	652	12.8	1040	12.6	2710	14.2
L mPSTs	11.7	5.31	34.5	4.58	85.9	3.91	197	3.85	361	4.35	698	3.66
R mPSTs	11.3	5.13	34.5	4.58	87.9	4.00	197	3.86	351	4.22	672	3.52
L mPSTp	0.420	0.191	1.22	0.161	3.97	0.181	4.48	0.088	8.80	0.106	10.8	0.057
R mPSTp	0.432	0.197	1.14	0.151	4.47	0.204	4.92	0.096	9.64	0.116	13.3	0.069
L mPTd	42.5	19.3	131	17.4	425	19.4	1020	19.9	1560	18.8	3640	19.1
R mPTd	40.0	18.2	135	17.9	427	19.4	1030	20.1	1590	19.2	3820	20.0
L mPTv	6.71	3.05	29.3	3.90	68.5	3.11	172	3.37	323	3.90	701	3.67
R mPTv	6.23	2.83	30.0	3.97	75.0	3.41	177	3.47	332	4.01	694	3.63
L mDM	7.76	3.53	24.1	2.57	105	3.83	330	5.18	340	4.11	674	3.53
R mDM	7.53	3.43	25.5	2.72	111	4.07	326	5.13	336	4.06	729	3.81

Alligator specimens are listed at the top, with skull length given below (increasing from left to right). Force is given in absolute values (N) and as a percentage of total force. Muscle abbreviations are as in Materials and methods: L, left; R, right. PCSA, physiological cross-sectional area.

models (Davis et al., 2010; Santana et al., 2010), our alligator models faithfully perform within an acceptable range of *in vivo* bite force. The good performance of the model further demonstrates the utility of high-fidelity muscle inputs. However, bite force in most individuals differed somewhat from predicted *in vivo* bite forces from similarly sized animals. These differences between *in silico* and *in vivo* techniques shed light on the challenges of modeling complex feeding function and cranial biomechanics. Causes for this mismatch may be divided into (1) differences between modeled bites and *in vivo* bites and (2) submaximal model performance.

First, the mechanism of bite force production in our models differs from the direct measurements of Erickson et al. (2003). Whereas we modeled static, crushing bites, Erickson et al. (2003) included some unknown amount of momentum: the maximum force during 'aggressive, snapping' bites. Therefore, the peak force reported by these authors likely included some degree of impact force resulting from rapid mandibular deceleration. Daniel and McHenry (2001) suggested that 'dynamic loading due to rapid deceleration' likely plays a role in maximal forces experienced by the skull. Because the present study modeled static, crushing bites, which have no momentum contribution from impact forces, estimated maximum bite forces are presumably below peak forces experienced by the cranium.

Second, the modeling techniques employed here underestimate the force of mPTv because models do not adequately capture aponeurotic muscle attachments. Crocodylians have a complex tendinous skeleton among the adductor mandibulae and pterygoideus muscle bellies (Iordansky, 1964, 2000; Schumacher, 1973; Busbey, 1989) that is challenging to model. Traditional tomography techniques fail to image these tendons with enough reliability to create digital models. Because the tendinous attachments of mPTv are missing ('U-tendon' of Iordansky, 1964; 'pterygoideus-tendon aponeuroses' of Schumacher, 1973; 'posterior pterygoid tendon' of Busbey, 1989), we underestimate the total surface area of muscle attachment and thus the total estimated force. mPTv accounts for approximately one-third of *A. mississippiensis* jaw muscle mass (Busbey, 1989; Cleuren et al., 1995) but only about 3% of the total muscle force in our model (Table 2). Moreover, the methods employed in this study place force vectors directly between attachment sites. mPTv originates on the edge of the pterygoid flange, courses caudoventrolaterally, then passes around the ventral border of the mandible to attach on the lateral surface of the angular bone. Force vectors oriented from muscle origin to insertion will therefore pass through the body of the mandible, resulting in erroneously collinear forces between the cranial and mandibular attachments of this muscle. Although BoneLoad

Table 3. Summary of *A. mississippiensis* bite forces calculated with 3D LM and FEA

Specimen	Skull length (cm)	Lever mechanics bite force (N)	FEA bite force (N)	% Difference	*In vivo* bite force (N)	% Error
AL 031	4.8	49.3	49.3	0	16.7	195
AL 622	9.9	150	146	2.70	122	21.3
AL 612	20.3	443	421	5.09	882	–51.0
AL 024	26.9	938	913	2.70	1913	–51.6
AL 700	33.3	1500	1470	2.02	3440	–56.8
AL 008	45.4	3460	3420	1.16	8070	–57.4

Note: finite element analysis (FEA) force presented here is dorsoventral force only; see Table 6 for bite force in all dimensions. 3D LM, three-dimensional lever mechanics.

Journal of Experimental Biology

Journal of Experimental Biology (2017) 220, 2036-2046 doi:10.1242/jeb.156281

Table 4. Muscle moments about jaw joint axis calculated with 3D LM

	M_{JJA} (N m)					
Muscle	AL 031 4.8 cm	AL 622 9.9 cm	AL 612 20.3 cm	AL 024 26.9 cm	AL 700 33.3 cm	AL 008 45.4 cm
L mAMES	0.033	0.372	1.44	4.47	9.22	28.5
R mAMES	0.037	0.355	1.48	5.05	8.92	25.6
L mAMEM	0.025	0.111	0.625	1.08	3.07	11.7
R mAMEM	0.025	0.107	0.592	1.23	3.03	9.65
L mAMEP	0.025	0.102	0.498	1.51	1.70	6.72
R mAMEP	0.025	0.098	0.460	1.49	1.71	6.30
L mAMP	0.114	0.837	4.94	15.8	24.9	108
R mAMP	0.127	0.755	4.50	15.5	23.9	96.1
L mPSTs	0.164	0.801	3.60	11.0	24.1	68.1
R mPSTs	0.154	0.829	3.63	11.6	23.5	66.2
L mPSTp	0.003	0.017	0.111	0.158	0.355	0.746
R mPSTp	0.003	0.016	0.117	0.180	0.400	0.885
L mPTd	0.141	0.809	6.24	16.4	30.3	119
R mPTd	0.128	0.755	4.83	16.9	30.5	120
L mPTv	0.027	0.247	1.28	3.98	10.8	29.5
R mPTv	0.025	0.241	1.42	3.99	14.2	31.5
L mDM	−0.025	−0.139	−0.692	−4.08	−6.30	−16.2
R mDM	−0.024	−0.162	−0.910	−3.95	−6.29	−18.6

Alligator specimens are listed at the top, with skull length given below (increasing from left to right). Muscle abbreviations are as in Materials and methods: L, left; R, right.

accounts for muscle fibers that pull on a curved surface of bone (‘muscle wrapping’ *sensu* Grosse et al., 2007), it does not account for subsequent changes to the course of a muscle fibers, such as occur when a muscle passes around a bone or other structure. We suggest that the former phenomenon (muscle forces distributed across a curved attachment surface) be called ‘muscle traction’ and the latter anatomical phenomenon be called ‘muscle wrapping’. To better reconstruct muscle function accurately, future neontological studies could use contrast-enhanced CT imaging of soft tissues (Gignac et al., 2016) to facilitate the inclusion of the tendinous skeleton and associated musculature as well as properly orient force vectors in wrapping (Moazen et al., 2008; Gröning et al., 2013). However, tendons are rarely preserved in the fossil record, leaving studies of muscle function in extinct taxa to rely on inferential methods. As this method was developed to apply to fossil crocodylomorphs and other vertebrates, tendinous attachments were not included in muscle attachments.

Because mPTv makes up a sizeable proportion of jaw muscle mass (Busbey, 1989; Cleuren et al., 1995), errors in modeling this muscle may be particularly deleterious to model fidelity. To explore the effects of altering the magnitude and orientation of mPTv force on model performance, we used our largest specimen to calculate bite force under three additional scenarios. To orient the force vector of mPTv more correctly, we used DiceCT-based scans to determine the angles of insertion of mPTv on the lateral surface of the articular bone. We then oriented muscle force along this adjusted vector rather than towards the muscle’s cranial attachment site (Fig. 7). To account for the underestimated PCSA of mPTv, we scaled muscle force magnitude by the ratio of muscle force calculated for mPTv by Gignac and Erickson (2016) over that of our own mPTv for equivalently sized animals (approximately 5.25 times). Gignac and Erickson (2016) dissected cadaveric specimens to calculate PCSA. This is inapplicable to fossil taxa, but presumably yields more accurate PCSA data. We then

Table 5. Contribution of each muscle to M_{JJA} (and thus bite force) calculated with 3D LM

	AL 031 4.8 cm	AL 622 9.9 cm	AL 612 20.3 cm	AL 024 26.9 cm	AL 700 33.3 cm	AL 008 45.4 cm
Muscle	Proportion (% total moment)					
L mAMES	3.10	5.76	4.03	4.05	4.38	3.91
R mAMES	3.52	5.50	4.14	4.58	4.24	3.52
L mAMEM	2.35	1.72	1.75	0.977	1.46	1.60
R mAMEM	2.37	1.66	1.65	1.11	1.44	1.32
L mAMEP	2.34	1.59	1.39	1.37	0.807	0.922
R mAMEP	2.34	1.52	1.28	1.35	0.816	0.864
L mAMP	10.8	13.0	13.8	14.3	11.8	14.9
R mAMP	12.0	11.7	12.6	14.1	11.3	13.2
L mPSTs	15.5	12.4	10.1	10.0	11.4	9.35
R mPSTs	14.6	12.8	10.2	10.5	11.2	9.09
L mPSTp	0.295	0.264	0.310	0.143	0.169	0.102
R mPSTp	0.296	0.255	0.328	0.163	0.190	0.121
L mPTd	13.4	12.5	17.4	14.9	14.4	16.3
R mPTd	12.1	11.7	13.5	15.3	14.5	16.5
L mPTv	2.53	3.83	3.57	3.61	5.12	4.05
R mPTv	2.40	3.73	3.97	3.62	6.74	4.32

Note: mDM is not included in this calculation.

Journal of Experimental Biology (2017) 220, 2036-2046 doi:10.1242/jeb.156281

Table 6. Components of *A. mississippiensis* bite force calculated with FEA

Specimen	F_x (N)	F_y (N)	F_z (N)	F_{sum} (N)
AL 031	−5.46	49.3	13.4	51.3
AL 622	−8.07	146	50.7	155
AL 612	−8.16	421	122	438
AL 024	−154	913	272	965
AL 700	−282	1470	403	1550
AL 008	−469	3420	704	3520

x, *y* and *z* refer to force in the mediolateral, dorsoventral and rostrocaudal direction; F_{sum} is total force. All data are for low gape.

combined these orientation and magnitude variables. Bite force for the 45.4 cm-long specimen was originally 3200 N. Reorienting mPTv force raised bite force to 3377 N, while scaling its force by 5.25 raised bite force to 4160 N. Combined, these effects resulted in a bite force of 4515 N. Both models in which mPTv force was scaled up resulted in substantially higher bite force. Of course, both sources of correctional data would be unavailable without access to fresh cadaveric specimens. Because a primary goal of this study was to develop a method with applicability to the fossil record, we present these results but do not incorporate them into the broader workflow or statistical analysis in this paper.

The prospect of 3D musculoskeletal cranial biomechanics

An integrative understanding of the feeding apparatus requires an accurate, comprehensive characterization of muscular inputs and their concomitant impacts on joint and cranial function. 3D computational analysis of musculoskeletal behavior is time intensive; however, these techniques allow researchers to investigate performance in conditions and numbers that cannot be replicated *in vivo*. Researchers are able to visualize muscle resultants and cranial forces in three dimensions, correlate muscle inputs with cranial performance, and uncover loading environments of key cranial structures such as jaw joints and sutures. This modeling workflow can assess each muscle's contribution to various cranial forces, characterize joint reaction force magnitude and orientation to better understand the gross anatomical and microanatomical adaptations joints have to loading environment, and investigate intracranial joints, secondary craniomandibular joints and dual joint systems. The jaw joint minimally resists all dorsoventrally oriented input forces that do not contribute to bite force. As such, it plays a key role in modulating and dispersing forces in the feeding apparatus. We would expect that the jaw joint will have a tissue composition that is well suited to its loading regime. Therefore, biomechanical studies and histological investigations can provide reciprocal illuminations into how joint morphology and composition correlate with loading environment.

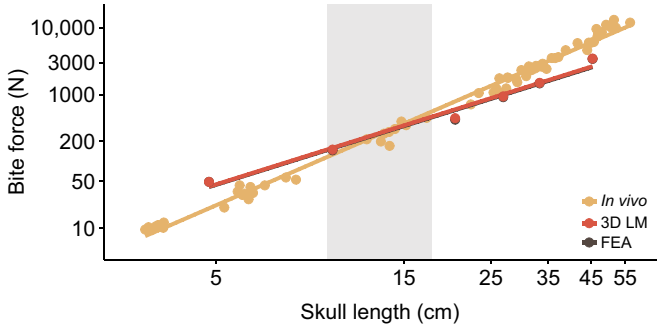

Fig. 6. Regression analysis of modeled and *in vivo* bite forces against skull length. The gray box indicates the region in which there is no significant difference in slope between calculated and *in vivo* bite force. *In vivo* data: Erickson et al., 2003. Modeled data: 3D LM, three-dimensional lever mechanics; FEA, finite element analysis.

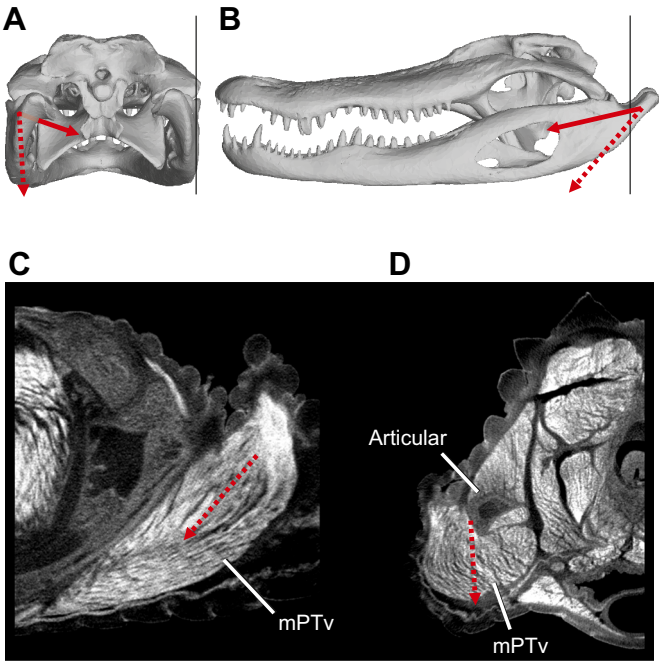

Fig. 7. Reorientation of mPTv force with DiceCT data. Solid arrow represents the original, attachment-based orientation of mPTv force; dashed arrow shows the reoriented force. (A) Caudal view of 45.4 cm skull length specimen. Vertical line represents the parasagittal slice shown in C. Transparent portion of arrow illustrates how original orientation of mPTv force clips through mandible. (B) Left lateral view of the same specimen. Vertical line represents the axial slice shown in D. (C) Parasagittal slice through mPTv. (D) Axial slice through mPTv. Note the muscle wrapping around the articular bone.

Evolution of the crocodylian skull

The 3D modeling approaches used in this study are well suited for application to the fossil record. Because these techniques use the area of muscle attachment site rather than the weight of dissected muscles to estimate PCSA, they can be used to make accurate estimates of muscle force, moments about axes and reaction forces in extinct animals. Effective use of osteological correlates (Holliday, 2009) and the extant phylogenetic bracket (Witmer, 1995; Holliday and Witmer, 2007) can constrain reconstructions of muscle attachment location, size and shape. Extant relatives can also inform the reconstruction of myological parameters such as pennation angle and fiber length.

The evolution of the modern crocodylian skull involved substantial changes to the skull (Langston, 1973; Busbey, 1995). In contrast to the platyrostral skulls of crocodylians, the earliest members of crocodylian-line archosaurs had oreinirostral skulls, such as the rauisuchian *Postosuchus* (Chatterjee, 1985) and the sphenosuchian *Sphenosuchus* (Walker, 1990). In these animals, the skull is dorsoventrally deep and mediolaterally narrow. The quadrates were dorsoventrally oriented (Walker, 1990) and, at least in sphenosuchians, were still not rigidly sutured to the braincase (Langston, 1973). A mobile suspensorium alongside an open palatobasal joint (Langston, 1973; Busbey, 1995) has been interpreted as evidence that these early ancestors of crocodylians

were kinetic (Walker, 1990). The evolution of the crown group therefore involved substantial reorientation of adductor muscles along with a reduction in kinetic potential. The transformation from oreinirostry to platyrostry presumably required crocodylians to evolve higher mass or pennation of adductor muscles to achieve equivalent bite forces to their fossil ancestors.

The biomechanical origins of the pterygoid buttress are also poorly understood. In crocodylians, the pterygoid buttress articulates with the medial surface of the mandible in what has been described as an 'open' or 'sliding' joint (Schumacher, 1973). Some researchers have hypothesized that it braces the mandible against 'reverse-wishboning' (Iordansky, 1964; Schumacher, 1973; Busbey, 1995). Porro et al. (2011) included the pterygoid buttress as a constraint of the mandible. Recently, the pterygoid buttress has been suggested to represent a key innovation underlying the crocodylian feeding apparatus (Holliday et al., 2015). Although mediolaterally acting muscle forces will cancel out when symmetrically recruited, they will load structures on which they act. In crocodylians and other taxa with substantial mediolateral components to muscle force, these forces are likely to be a primary source of stress in the skull.

The loss of cranial kinesis along with the elaboration of the pterygoid flange into a novel craniomandibular articulation represent key features of crocodylian evolution (Holliday et al., 2015). Indeed, many of the hallmark features of the crocodylian skull, including an expanded retroarticular process, laterally attaching pterygoideus muscles, a bony secondary palate and broad scarf joints followed the evolution of the pterygoid buttress. The methods used in this paper will be applied to assess the kinetic status of fossil relatives of crocodylians and to investigate the role of the pterygoid buttress in the feeding apparatus of these derived archosaurs.

Conclusions

This study is one of the first to use both 3D LM and FEA to investigate the production of bite force in an ontogenetic series of *A. mississippiensis*. The use of anatomically accurate muscle attachments is key to the success of the models, and the good agreement between the two methods lends support to these techniques. The modeling techniques in this study can be used to assess the effect of changing muscle size and orientation during the evolution of the modern crocodylian skull. Key features of the crocodylian skull may have permitted novel muscular morphologies. These methods will allow researchers to test hypotheses linking bony features such as the loss of kinesis, secondary palate, scarf joints and the pterygoid buttress with muscular innovations, such as generally enlarged adductor mass, laterally inserting mPTv and the extensive cranial tendinous skeleton.

Acknowledgements

We thank Ruth Elsey and the staff of Rockefeller Wildlife Refuge for providing specimens. We thank the University of Missouri Biomolecular Imaging Center, the University of Missouri School of Medicine Department of Radiology and the University of Missouri School of Veterinary Medicine for scanning specimens. We thank Betsy Dumont, Larry Witmer, Laura Porro and Kent Vliet for helpful discussions. We thank two anonymous reviewers, whose comments greatly enhanced the quality and clarity of the manuscript.

Competing interests

The authors declare no competing or financial interests.

Author contributions

Conceptualization: K.C.S. and C.M.H.; Methodology: K.C.S., K.M.M., J.L.D. and C.M.H.; Software: K.C.S., K.M.M., J.L.D. and C.M.H.; Formal Analysis: K.C.S. and K.M.M.; Investigation: K.C.S.; Resources: K.M.M. and C.M.H.; Data Curation: K.C.S. and C.M.H.; Writing - Original Draft: K.C.S. and C.M.H.; Writing - Review and Editing: K.C.S., K.M.M., J.L.D. and C.M.H.; Visualization: K.C.S., K.M.M. and C.M.H.; Project Administration: K.C.S. and C.M.H.; Funding Acquisition: K.C.S., K.M.M., J.L.D. and C.M.H.

Funding

This research was supported by the National Science Foundation (IOS 1457319 and EAR 1631684), the University of Missouri Research Board, the University of Missouri Research Council and the University of Missouri Department of Pathology and Anatomical Sciences.

Data availability

Data are available from Open Science Framework: https://osf.io/jmpck/

Supplementary information

Supplementary information available online at
http://jeb.biologists.org/lookup/doi/10.1242/jeb.156281.supplemental

References

Bates, K. T. and Falkingham, P. L. (2012). Estimating maximum bite performance in *Tyrannosaurus rex* using multi-body dynamics. *Biol. Lett.* **8**, 660-664.

Busbey, A. B. (1989). Form and function of the feeding apparatus of *Alligator mississippiensis*. *J. Morphol.* **202**, 99-127.

Busbey, A. B. (1995). The structural consequences of skull flattening in crocodilians. In *Functional Morphology in Vertebrate Paleontology* (J. J. Thomason), pp. 173-192. Cambridge: Cambridge University Press.

Chatterjee, S. (1985). *Postosuchus*, a new thecodontian reptile from the triassic of texas and the origin of tyrannosaurs. *Philos. Trans. R. Soc. Lond.* **309**, 395-460.

Cleuren, J. and de Vree, F. (1992). Kinematics of the jaw and hyolingual apparatus during feeding in *Caiman crocodilus*. *J. Morphol.* **212**, 141-154.

Cleuren, J., Aerts, P. and De Vree, F. (1995). Bite and joint force analysis in *Caiman crocodilus*. *Belg. J. Zool.* **12**, 79-94.

Curtis, N., Jones, M. E. H., Evans, S. E., O'Higgins, P. and Fagan, M. J. (2013). Cranial sutures work collectively to distribute strain throughout the reptile skull. *J. R. Soc. Interface* **10**, 1-9.

Daniel, W. J. T. and McHenry, C. (2001). Bite force to skull stress correlation—modelling the skull of *Alligator mississippiensis*. In *Crocodilian Biology And Evolution* (ed. G. C. Grigg, F. Seebacher and C. Franklin), pp. 135-143. Chipping Norton, NSW: Surrey Beatty and Sons.

Davis, J. L., Santana, S. E., Dumont, E. R. and Grosse, I. R. (2010). Predicting bite force in mammals: two-dimensional *versus* three-dimensional models. *J. Exp. Biol.* **213**, 1844-1851.

Erickson, G. M., Lappin, A. K. and Vliet, K. A. (2003). The ontogeny of bite-force performance in American alligator (*Alligator mississippiensis*). *J. Zool.* **260**, 317-327.

Erickson, G. M., Gignac, P. M., Steppan, S. J., Lappin, A. K., Vliet, K. A., Brueggen, J. D., Inouye, B. D., Kledzik, D. and Webb, G. J. W. (2012). Insights into the ecology and evolutionary success of crocodilians revealed through bite-force and tooth-pressure experimentation. *PLOS ONE* **7**, e31781.

Erickson, G. M., Gignac, P. M., Lappin, A. K., Vliet, K. A., Brueggen, J. D. and Webb, G. J. W. (2014). A comparative analysis of ontogenetic bite-force scaling among Crocodylia. *J. Zool.* **292**, 48-55.

Gans, C. (1982). Fiber architecture and muscle function. *Exerc. Sports Sci. Rev.* **10**, 160-207.

Gignac, P. M. and Erickson, G. M. (2015). Ontogenetic changes in dental form and tooth pressures facilitate developmental niche shifts in American alligators. *J. Zool.* **295**, 132-142.

Gignac, P. M. and Erickson, G. M. (2016). Ontogenetic bite-force modeling of *Alligator mississippiensis*: implications for dietary transitions in a large-bodied vertebrate and the evolution of crocodylian feeding. *J. Zool.* **299**, 229-238.

Gignac, P. M., Kley, N. J., Clarke, J. A., Colbert, M. W., Morhardt, A. C., Cerio, D., Cost, I. N., Cox, P. G., Daza, J. D., Early, C. M. et al. (2016). Diffusible iodine-based contrast-enhanced computed tomography (diceCT): an emerging tool for rapid, high-resolution, 3-D imaging of metazoan soft tissues. *J. Anat.* **228**, 889-909.

Gröning, F., Jones, M. E. H., Curtis, N., Herrel, A., O'Higgins, P., Evans, S. E. and Fagan, M. J. (2013). The importance of accurate muscle modelling for biomechanical analyses: a case study with a lizard skull. *J. R. Soc. Interface* **10**, 20130216.

Grosse, I. R., Dumont, E. R., Coletta, C. and Tolleson, A. (2007). Techniques for modeling muscle-induced forces in finite element models of skeletal structures. *Anat. Rec.* **290**, 1069-1088.

Holliday, C. M. (2009). New insights into dinosaur jaw muscle anatomy. *Anat. Rec.* **292**, 1246-1265.

Holliday, C. M. and Witmer, L. M. (2007). Archosaur adductor chamber evolution: integration of musculoskeletal and topological criteria in jaw muscle homology. *J. Morphol.* **268**, 457-484.

Holliday, C. M., Tsai, H. P., Skijan, R. J., George, I. D. and Pathan, S. (2013). A 3D interactive model and atlas of the jaw musculature of *Alligator mississippiensis*. *PLOS ONE* **8**, e62806.
Holliday, C. M., Sellers, K. C., Vickaryous, M. K., Ross, C. F., Porro, L. B., Witmer, L. M. and Davis, J. L. (2015). The functional and evolutionary significance of the crocodyliform pterygomandibular joint. *Integr. Comp. Biol.* **55** suppl. 1, e81.
Iordansky, N. N. (1964). The jaw muscles of the crocodiles and some relating structures of the crocodilian skull. *Anat. Anz.* **115**, 256-280.
Iordansky, N. N. (1973). The skull of the Crocodilia. In *Biology of the Reptilia*, Vol. 4 (ed. C. Gans and T. S. Parsons). pp. 263-289. London: Academic Press.
Iordansky, N. N. (2000). Jaw muscles of the crocodiles: structures, synonymy, and some implications of homology and functions. *Russ. J. Herpetol.* **7**, 41-50.
Johnson, P. O. and Neyman, J. (1936). Tests of certain linear hypotheses and their application to some educational problems. *Stat. Res. Memoirs* **1**, 57-93.
Langston, W. (1973). The crocodilian skull in historical perspective. In *Biology of the Reptilia*, vol. 4, (ed. C. Gans and T. S. Parsons), pp. 263-289. London: Academic Press.
McCurry, M. R., Evans, A. R. and McHenry, C. R. (2015). The sensitivity of biological finite element models to the resolution of surface geometry: a case study of crocodilian crania. *PeerJ* **3**, e988.
McHenry, C. R., Clausen, P. D., Daniel, W. J. T., Meers, M. B. and Pendharkar, A. (2006). Biomechanics of the rostrum in crocodilians: a comparative analysis using finite-element modeling. *Anat. Rec. A Discow. Mol. Cell Evol. Biol.* **288**, 827-849.
Metzger, K. A. and Herrel, A. (2005). Correlations between lizard cranial shape and diet: a quantitiative, phylogenetically informed analysis. *Biol. J. Linn. Soc.* **86**, 433-466.
Metzger, K. A., Daniel, W. J. T. and Ross, C. F. (2005). Comparison of beam theory and finite-element analysis with in vivo bone strain data from the alligator cranium. *Anat. Rec. A Discow. Mol. Cell Evol. Biol.* **283**, 331-348.
Molnar, R. E. (1998). Mechanical factors in the design of the skull of *Tyrannosaurus rex* (Osborn, 1905). *Gaia* **15**, 193-218.
Moazen, M., Curtis, N., Evans, S. E., O'Higgins, P. and Fagan, M. J. (2008). Combined finite element and multibody dynamics analysis of biting in a *Uromastyx hardwickii* lizard skull. *J. Anat.* **213**, 499-508.
Pierce, S. E., Angielczyk, K. D. and Rayfield, E. J. (2008). Patterns of morphospace occupation and mechanical performance in extant crocodilian skulls: a combined geometric morphometric and finite element modeling approach. *J. Morph.* **269**, 840-864.
Pierce, S. E., Angielczyk, K. D. and Rayfield, E. J. (2009). Shape and mechanics in thalattosuchian (Crocodylomorpha) skulls: implications for feeding behaviour and niche partitioning. *J. Anat.* **215**, 555-576.
Porro, L. B., Holliday, C. M., Anapol, F., Ontiveros, L. C., Ontiveros, L. T. and Ross, C. F. (2011). Free body analysis, beam mechanics, and finite element modeling of the mandible of *Alligator mississippiensis*. *J. Morphol.* **272**, 910-937.
Porro, L. B., Metzger, K. A., Iriarte-Diaz, J. and Ross, C. F. (2013). *In vivo* bone strain and finite element modeling of the mandible of *Alligator mississippiensis*. *J. Anat.* **223**, 195-227.
Rayfield, E. J. and Milner, A. C. (2008). Establishing a framework for archosaur cranial mechanics. *Paleobiology* **34**, 494-515.
Rayfield, E. J., Milner, A. C., Xuan, V. B. and Young, P. G. (2007). Functional morphology of spinosaur 'crocodile-mimic' dinosaurs. *J. Vertebr. Paleontol.* **27**, 892-901.
Sacks, R. D. and Roy, R. R. (1982). Architecture of the hind limb muscles of cats: functional significance. *J. Morphol.* **173**, 185-195.
Santana, S. E., Dumont, E. R. and Davis, J. L. (2010). Mechanics of bite force production and its relationship to diet in bats. *Funct. Ecol.* **24**, 776-784.
Schaerlaeken, V., Holanova, V., Boistel, R., Aerts, P., Velensky, P., Rehak, I., Andrade, D. V. and Herrel, A. (2012). Built to bite: feeding kinematics, bite forces, and head shape of a specialized durophagous lizard, dracaena guianensis (Teiidae). *J. Exp. Zool.* **317A**, 371-381.
Schumacher, G.-H. (1973). The Head Muscles and Hyolaryngeal Skeleton of Turtles and Crocodilians. In *Biology of the Reptilia*, vol. 4, (ed. C. Gans and T. S. Parsons), pp. 101-199. London: Academic Press.
Sinclair, A. G. and Alexander, R. M. (1987). Estimates of forces exerted by the jaw muscles of some reptiles. *J. Zool. Soc. Lond.* **213**, 107-115.
Strait, D. S., Wang, Q., Dechow, P. C., Ross, C. F., Richmond, B. G., Spencer, M. A. and Patel, B. A. (2005). Modeling elastic properties in finite element analysis: how much precision is needed to produce an accurate model? *Anat. Rec. A Discow. Mol. Cell Evol. Biol.* **283A**, 275-287.
Tseng, Z. J. and Stynder, D. (2011). Mosaic functionality in a transitional ecomorphology: skull biomechanics in stem Hyaeninae compared to modern South African carnivorans. *Biol. J. Linn. Soc.* **102**, 540-559.
Van Drongelen, W. and Dullemeijer, P. (1982). The feeding apparatus of *Caiman crocodilus*; a functional-morphological study. *Anat. Anz.* **151**, 337-366.
Walker, A. D. (1990). A revision of *sphenosuchus acutus* haughton, a crocodylomorph reptile from the elliot formation (late triassic or early jurassic) of south africa. *Philos. Trans. Biol. Sci.* **330**, 1-120.
White, C. R. (2003). Allometric analysis beyond heterogeneous regression slopes: use of the johnson-neyman technique in comparative biology. *Physiol. Biochem. Zool.* **76**, 135-140.
Witmer, L. M. (1995). The extant phylogenetic bracket and the importance of reconstructing soft tissues in fossils. In *Functional Morphology in Vertebrate Paleontology* (ed. J. Thomason), pp. 19-33. Cambridge: University Press.
Woodward, A. R., White, J. H. and Linda, S. B. (1995). Maximum size of the alligator (*Alligator mississippiensis*). *J. Herpetol.* **29**, 507-513.
Zapata, U., Metzger, K., Wang, Q., Elsey, R. M., Ross, C. F. and Dechow, P. C. (2010). Material properties of mandibular cortical bone in the American alligator, *Alligator mississippiensis*. *Bone* **46**, 860-867.